Spatially Selective Holographic Photoactivation and Functional Fluorescence Imaging in Freely Behaving Mice with a Fiberscope

Vivien Szabo, Cathie Ventalon, Vincent de Sars, Jonathan Bradley, Valentina Emiliani

Spatially selective photoactivation with computer generated holography and functional fluorescence imaging in freely behaving mice with a fiberscope

Vivien Szabo*[1], Cathie Ventalon*[1], Vincent De Sars[1], Jonathan Bradley[2], and Valentina Emiliani[1]

(1) Wavefront-Engineering Microscopy Group, Neurophotonics Laboratory, Centre National de la Recherche Scientifique UMR8250, Université Paris Descartes, 45 Rue des Saints Pères, F-75006 Paris, France

(2) Laboratoire de Physiologie Cérébrale, Centre National de la Recherche Scientifique UMR8118, Université Paris Descartes, 45 Rue des Saints Pères, F-75006 Paris, France

*these authors contributed equally to the work

Contact: valentina.emiliani@parisdescartes.fr

Running title: Patterned photoactivation in freely behaving mice

Summary

Correlating patterned neuronal activity to defined animal behaviors is a core goal in neuroscience. Optogenetics is one large step toward achieving this goal, yet optical methods to control neural activity in behaving rodents have thus far been limited to perturbing all light-sensitive neurons in a large volume. Here, we demonstrate an all-optical method for precise spatial control and recording of neuronal activity in anesthetized and awake freely behaving mice. Photoactivation patterns targeted to multiple neuronal somata, produced with computer-generated holography, were transmitted to the mouse brain using a micro-objective coupled fiber bundle. Fluorescence imaging through the same device, via epifluorescence, structured illumination, or scanless multipoint confocal microscopy, allowed imaging neurons and recording neuronal activity. The fiberscope was tested in mice co-expressing ChR2-tdTomato and GCaMP5-G

in cerebellar interneurons, delivering near-cellular resolution photoactivation in freely behaving mice.

Highlights:

- A novel fiberscope for optogenetics in freely behaving mice
- Photoactivation with near-cellular resolution using computer generated holography
- Functional fluorescence imaging with optical sectioning
- Combined ChR2 photoactivation and functional calcium recording in the same neurons

INTRODUCTION

Optogenetics enables light to control and monitor complex computational events in the brain through targeted perturbation of neuronal circuits and imaging of functional reporters (Akerboom et al., 2013; Deisseroth, 2011; Miesenboeck, 2011). Neuron-specific expression and light sensitivity of optogenetics tools, including a growing list of new opsins (Klapoetke et al., 2014; Lin et al., 2013) permit efficient and selective control of neuronal networks with relatively simple optical methods (Aravanis et al., 2007; Huber et al., 2008; Kitamura et al., 2014). The fascinating prospect of optically orchestrating neuronal circuitry in awake freely behaving rodents calls for the development of more sophisticated illumination schemes. Ideally these methods should allow activation of targeted sets of individual neurons with variable (user-defined) shape, millisecond resolution and minimal invasiveness.

Reduction of illumination volume in order to stimulate a single neuron can be achieved by guiding excitation light through fiber-optic based microprobes (LeChasseur et al., 2011) or by scanning a laser beam coupled to a microscope objective (Packer et al., 2012; Prakash et al., 2012; Wilson et al., 2012) or a fiber bundle (Hayashi et al., 2012). This permits *in vivo* targeting with cellular (LeChasseur et al., 2011; Prakash et al., 2012) or near-cellular (Hayashi et al.,

2012; Wilson et al., 2012) resolution in anesthetized mice. Multineuronal excitation with these approaches, however, remains challenging. Targeting of multiple neurons with individual fiber-optic microprobes (LeChasseur et al., 2011) requires implanting multiple separate probes, thus limiting the maximum number of neurons that can be stimulated in a given volume. Scanning approaches (Hayashi et al., 2012; Prakash et al., 2012; Wilson et al., 2012) are more flexible but because they rely on sequential photoactivation of multiple targets they degrade temporal resolution. Furthermore, none of these methods have yet been demonstrated in freely moving rodents.

Neuronal activation at multiple sites simultaneously can be achieved by implanting an array of fiber probes (Kim et al., 2013; Royer et al., 2010; Stark et al., 2012; Zorzos et al., 2012) or optical fibers with multiple light windows (Pisanello et al., 2014). However because the geometry of the probe array imposes a fixed distance between photoactivation sites, the stimulation patterns have limited flexibility, and, among the few demonstrations reported, they have yet to approach neuron resolution in freely behaving mice (Kim et al., 2013; Stark et al., 2012). Moreover, these methods remain to be combined with functional imaging.

Simultaneous excitation of multiple neurons with single cell resolution can be achieved by shaping the excitation volume by intensity modulation using digital micromirror devices (DMD) (Dhawale et al., 2010), or by phase modulation techniques such as computer-generated holography (CGH) or generalized phase contrast using liquid crystal displays (Lutz et al., 2008; Papagiakoumou et al., 2010). Based on these approaches, efficient photoactivation of single or multiple neurons in brain slices (Lutz et al., 2008; Papagiakoumou et al., 2010) or in living mice (Dhawale et al., 2010) is possible. Neither these methods however have yet been extended to freely behaving rodents.

Here, we present a fiberscope capable of spatially selective illumination in freely behaving mice, achieved by coupling an optical microscope for CGH to a fiber

bundle tipped with a micro-objective. Each individual fiber core in the bundle permits stable and efficient transmission of one pixel of the CGH intensity pattern into the brain. The fiber bundle is also coupled to a versatile imaging system that permits, through the use of a DMD, fluorescence imaging with different modalities comprising widefield epifluorescence, structured illumination and multipoint confocal imaging. This imaging system is used to locate neurons to design photoactivation patterns and to record neuronal activity following photoactivation.

Proof of principle experiments were conducted in cerebellar molecular layer interneurons co-expressing GCaMP5-G and ChR2-tdTomato in both anesthetized and freely behaving mice. By combining CGH with multipoint confocal microscopy we found conditions that minimize ChR2 photoactivation during imaging, allowing simultaneous photostimulation and functional imaging with near-cellular resolution.

Our new method permits the control and monitoring of circuit dynamics in freely behaving mice with unprecedented spatial precision, significantly extending the toolbox for investigation of neural microcircuits underlying signal processing and behavior.

RESULTS

The optical system comprises two distinct optical paths for holographic photoactivation and fluorescence imaging (Figure 1A and S1A). Holographic photoactivation was achieved with a liquid crystal spatial light modulator (LC-SLM), which phase-modulates a 473nm laser beam using CGH (Lutz et al., 2008; Zahid et al., 2010) to generate user specified patterns of various sizes and shapes (Figure 1B-C and Figure S1B-C). The lateral size and shape of the illumination pattern determine its axial extent, which is defined as the full-width at half maximum (FWHM) of the intensity profile along the optical axis. For circular shapes, the axial extent is about three times the spot diameter (Figure 1D-E). Therefore, to approach cellular resolution, photoactivation spots of 5µm

diameter and 18μm axial extent (Figure 1D) were used.

The fluorescence imaging system is fully described in SUPPLEMENTAL EXPERIMENTAL PROCEDURES. Briefly, a DMD, composed of a matrix of movable micromirrors, was illuminated by a 491nm laser beam (Figure 1A). The orientation of the micromirrors could be dynamically controlled to permit creation of different illumination patterns at the sample plane. Different imaging modalities could be achieved depending on the illumination pattern: epifluorescence, structured illumination (Bozinovic et al., 2008; Neil et al., 1997) or multipoint confocal microscopy (Figure 2). These modalities were used to record fluorescence signals of cerebellar interneurons from mice expressing GCAMP5 (Figure S2A). Conventional epifluorescence imaging (Figure 2B, left) was obtained by orienting all the micromirrors to the "on" position to project a uniform intensity pattern to the sample plane (Figure 2A, left pattern). Structured illumination microscopy (SIM) (Figure 2B, right) was achieved by controlling the orientation of the DMD micromirrors to illuminate the sample with a sequence of three shifted grids (Figure 2A, right pattern). Processing of the three corresponding images efficiently rejected out-of-focus light, which resulted in effective optical sectioning (see Figure S2B-C for the general principle of SIM) and better image contrast than with epifluorescence imaging. Axial resolution could be adjusted online according to experimental needs by simply changing the period of the illumination grid (Figure 2C). Finally, scanless multipoint confocal microscopy enabled fluorescence recordings from a chosen subset of points with high spatial resolution. This modality was obtained by adjusting the orientation of the DMD micromirrors to illuminate the sample with one or several small spots and then collecting the fluorescence from the corresponding regions of interest (ROIs) at the camera (Figure 2D-E). This is equivalent to a confocal microscope with a programmable array of pinholes allowing simultaneous fluorescence collection from multiple points. The corresponding point spread function (PSF), and therefore the lateral and axial resolutions achieved in this mode, depend on the size of the excitation spots and corresponding ROIs at the camera. By choosing excitations spots and ROIs of 4μm diameter, we obtained a PSF sufficiently small

to reach near cellular resolution, with lateral and axial resolutions of 3.1 and 8.6µm respectively (FWHM) (Figure 2F-G).

Photoactivation and imaging in anesthetized mice

To test photostimulation selectivity, we conducted photoactivation and calcium imaging *in vivo* in mice co-expressing GCaMP5-G (Akerboom et al., 2012) and ChR2-tdTomato in molecular layer interneurons (MLIs) in the most dorsal lobe (IV/V) of the cerebellar vermis (see, SUPPLEMENTAL EXPERIMENTAL PROCEDURES, Figure S2 and SUPPLEMENTAL RESULTS). Experiments were initially performed in anesthetized mice. Since ChR2 activation and GCaMP5-G excitation spectra overlap (Akerboom et al., 2012; Nagel et al., 2003), ChR2 photoactivation might be induced from the illumination light used for Ca^{2+} imaging. Therefore, in order to achieve a stable baseline fluorescence, GCaMP5-G imaging was done at a relatively low power density ($Pi \leq 0.5 mW/mm^2$) in the scanless confocal configuration so that only the soma(ta) of interest were illuminated (Figure 3A). Photoactivation consisted of 24 light pulses (60ms pulse duration at 9Hz), and the GCaMP5-G fluorescence signal was measured after each pulse (Figure 3B, bottom). With this protocol, we could reliably elicit an increase in GCaMP5-G fluorescence signal (Figure 3B, top trace) by targeting a single soma with a 5µm diameter photoactivation spot (power density $P=25 mW/mm^2$). In the absence of ChR2 expression, we found no change in GCaMP5-G fluorescence (mean $\Delta F/F_p$ = 0.1%, where $\Delta F/F_p$ is the calcium signal amplitude, see Figure 3B and SUPPLEMENTAL EXPERIMENTAL PROCEDURES; 95% confidence interval of the mean (CI95), [-0.7%; 0.9%]; $P=75 mW/mm^2$; n=48 cells from 3 mice) (Figure 3B, bottom trace). In ChR2/GCaMP5-G co-expressing neurons, the evoked signal rose linearly with the number of pulses, similar to previous observations at MLI soma with Fura-2 imaging in cerebellar slices (Franconville et al., 2011). Thus, each pulse drove a ChR2-mediated cation influx leading to an increase of GCaMP5-G fluorescence. After photoactivation, the signal decrease was approximated with a monoexponential decay (τ=0.96s) (CI95, [0.80s; 1.14s]; n=7 cells from 5 mice) (Figure 3B top trace), similar to (Akerboom et al., 2012). Photoactivation pulses as short as 5ms could also trigger functional responses (n=4 cells from 1 mouse)

(Figure S3), but the S/N ratio was too low to characterize the photoactivation resolution. Therefore, most experiments were performed with trains of 60ms pulses. This imaging/stimulation protocol reliably evoked calcium signals in cerebellar MLIs (120 cells from 9 mice, $\Delta F/F_p$>20%) and was highly repeatable in single neurons (Figure 3C).

We next characterized photoactivation resolution by quantifying the somatic GCaMP5-G response when the photoactivation spot was displaced off the soma, expressed as the ratio $R = (\Delta F/F_{p,\ off\ cell})/(\Delta F/F_{p,\ on\ cell})$ (Figure 4A). Resolution was first measured along the x-axis, orthogonal to the sagittal orientation of MLI dendrites (see inset of Figure 4A, left). In this way, processes or gap junctions connecting a stimulated MLI to other MLIs would not confound our measurement of lateral resolution (Kim et al., 2014; Rieubland et al., 2014). When the photoactivation spot was moved ~7μm from the center of the soma, the calcium signal was reduced by a factor of 2, and vanished when the spot was 20μm away ($R= -9 \times 10^{-3}$; CI95 [-7.1×10^{-2}; 5.3×10^{-2}]; n=14 cells from 7 mice) (Figure 4A, left). When the spot was moved along the sagittal orientation y (Figure 4A, right and Figure S4B) the lateral resolution significantly deteriorated (~30μm HWHM).

Experimentally characterizing the axial selectivity of photoactivation requires decoupling the imaging plane from the photostimulation plane. To do this characterization, we measured the calcium signal from a chosen soma at a fixed plane (z_0) while targeting different locations above the soma (z) by displacing the fiberscope probe (and therefore the photoactivation plane) with a piezoelectric device. The photoactivation protocol was a single 1s duration pulse. We benefited from the fact that the calcium signal lasts for >1s after the photoactivation beam is turned off so that the fiberscope probe could be placed back at z_0 after the photostimulation protocol and the calcium response from the soma still could be recorded. The response was reduced by a factor of 2 for photostimulation at z≈35μm (Figure 4A, middle). These results show that a near-cellular resolution can be obtained when targeting a single cell.

The measured lateral and axial photoactivation resolutions were compared with the expected resolutions in the ideal case where there is no scattering and where only the soma is labeled. The latter was obtained by calculating the convolution between the measured 3D intensity profile of the 5µm diameter spots used for photostimulation (Figure 1C) and a sphere of 7 µm in diameter representing the soma (see SUPPLEMENTAL EXPERIMENTAL PROCEDURES for details). The results are plotted along with the experimental data (Figures 4A, right). We found expected lateral and axial resolutions of 5µm and 14µm (HWHM) respectively. Therefore, when the photostimulation spot was moved perpendicular to the plane containing the dendrites, the measured lateral resolution (~7µm HWHM) was close to the expected resolution of ~5µm HWHM. This confirmed that the spot shape is well conserved in the photoactivation plane, and that scattering does not significantly degrade the resolution. However, when the photostimulation spot was moved along the dendritic plane, the experimental lateral resolution (~30µm HWHM) significantly differed from the expected one (~5µm HWHM). Similarly, when the spot was moved above the soma, in the plane containing the dendrites, the measured axial resolution (~35µm HWHM) significantly differed from the expected one (~14µm HWHM). Overall these finding suggest that the main source for resolution broadening comes from photoactivation of distal dendritic or axonal processes.

In order to confirm our ability to photostimulate a single neuron, we monitored the activity of 5 neurons simultaneously while targeting only one of these neurons for photoactivation (Figure 4B, left). A response was indeed observed only in the targeted cell (signal remaining in a non-targeted cell was $R = 6 \times 10^{-3}$ (CI95 [-1.4×10^{-2}; 2.6×10^{-2}]; n=27 neurons from 6 mice; see SUPPLEMENTAL EXPERIMENTAL PROCEDURES) (Figure 4B left).

Using CGH, multiple neurons can be targeted simultaneously for photostimulation, by placing one photoactivation spot on each soma. However, a limitation in photoactivation resolution arises when increasing the number of

photoactivation spots. Indeed, this results in an increased photoactivation power that might cause out-of-focus dendritic excitation. For this reason lateral selectivity was tested while several (5) neurons were photoactivated simultaneously. We first targeted the 5 neurons, eliciting a calcium signal in each soma (Figure 4B, center). We then displaced one of the five photoactivation spots by 20µm along the x-axis (perpendicular to the dendritic planes), which led to a considerable decrease in the corresponding neuronal response (R = 0.16; CI95 [0.096; 0.23]; n= 26 cells from 5 mice) (Figure 4B, right). This registration of calcium response to targeted neuron shows that cellular level resolution is maintained with our fiberscope even when simultaneously photoactivating a subpopulation of ChR2-expressing neurons. Notably, near-cellular resolution is maintained even when targeted cells were separated by ~20µm (Figure S4C).

Photoactivation and imaging in freely behaving mice

We then tested the fiberscope in freely behaving mice. The fiberscope probe was fixed to the mouse skull with a custom-made head-plate and holder (1.1g mass including adhesives and screws, Figure 5A and Figure S5A), allowing fluorescence imaging in the awake mouse (Figure 5B-C and Figure S5B). Normal exploration, eating, gnawing, grooming, jumping and sleeping behaviors were observed during the experimental sessions (up to 8 hours). With awake freely-behaving mice, movement can occur between the fiberscopic probe and the observed region of the brain. We studied this movement in two different types of mice: the same mice co-expressing GCaMP5-G and ChR2-tdTomato in cerebellar MLIs as used above for the anesthetized experiments, and mice bred heterozygous for both Pcp2-cre (Barski et al., 2000) and Rainbow (Tabansky et al., 2013) expressing eYFP in a random subset of cerebellar Purkinje cells. Movements were measured on 2 different timescales. The position of the observed cerebellar region was first monitored at 19Hz during a 100s epoch (Figure 5D-E and Movie S1). On average, the movement amplitude was Δx=1.6µm and Δy=1.2µm (n=30 acquisitions from 3 mice) (Figure 5E). Overall, the maximum movement in x or y during a 100s period was <3µm. Therefore, similarly to other fiberscope implementations (Flusberg et al., 2008; Kerr and

Nimmerjahn, 2012), the observed region remained stable during experimental epochs. This allowed repetitive stimulation of the same neuron, with simultaneous recording of the evoked functional response, without needing to reposition the photoactivation and imaging spots. Over 200 minutes, we recorded a mean translation and rotation of the field of view of Δx=8μm, Δy=5μm, $\Delta\theta$=2° (n = 6 mice) (Figure 5F-G, Figure S5C, Movie S2). Because our approach permits image acquisition, such lateral displacements can be easily corrected during prolonged experiments by acquiring new SIM images and refreshing the photostimulation and confocal imaging patterns on the SLM and DMD, respectively.

The same imaging/photoactivation protocol to photoactivate single somata used in anesthetized mice was repeated in freely behaving mice coexpressing GCaMP5-G and ChR2-tdTomato in cerebellar MLIs. Calcium signals could be similarly elicited in the targeted cells (Figure 6A), with a GCaMP5-G calcium transient decay time of τ=0.81s (CI95 [0.67s; 0.94s]; n=28 cells from 3 mice). We tested a few illumination light intensities and found that a light dose between 50 and 75mW/mm^2, corresponding to <1.5μW per illuminated neuron, resulted in a ΔF/F>10% in most cells, i.e., 39 of 44 cells chosen randomly in the fields of view of 4 freely behaving mice were responsive ($\Delta F/F_p$ >10%) and 5 were nonresponsive ($\Delta F/F_p$ <10%). This working light dose is in the range used in previous experiments (1-250μW/cell) (Dhawale et al., 2010; Lim et al., 2012; Madisen et al., 2012; Petreanu et al., 2007) and significantly lower than the reported photodamage threshold (>500μW/cell) (Petreanu et al., 2007).

Single neuron photoactivation assays were conducted in freely behaving mice. The lateral selectivity of photoactivation (Figure 6B and Movie S3) was comparable to the one measured in anesthetized mice (Figure 4A, left). Indeed, in freely behaving animals, the remaining signal when the spot was displaced by 20μm along the x-axis (perpendicular to the dendritic plane) was R= 8.1 x 10^{-2} (CI95 [2.7x 10^{-2}; 1.3 x 10^{-1}]; n=18 cells from 5 mice), with a lateral resolution of approximately 10μm (HWHM). To confirm overall stability of photoactivation

and imaging in the behaving mouse, we repeated our photoactivation protocol every 30s for 15 minutes without repositioning the photoactivation spot. In this case a calcium signal was evoked every time, confirming that there was not significant displacement of the field of view that might affect our ability to target a neuron (n=3 cells from 1 mouse) (Figure 6C and movie S4).

In 32 of 52 photoactivated neurons ($\Delta F/F_p$ >10%, P=25-75mW/mm^2) in the aforementioned 5 freely behaving mice, we also observed fluorescence transients (Figure 6C and Figure S6) in the time interval between two stimuli, i.e., not evoked by the photostimulation light. These transients were not observed in anesthetized mice. The small x-y movements observed (as discussed above) and the finding that the observed transients were always positive suggest that they were not due to movement artifact. Besides, it is unlikely that these transients were evoked by the imaging light since the photoactivation threshold is unchanged if not higher in awake than in anesthetized animals (range of photoactivation power densities used for all experiments: P_{awake} = [25mW/mm^2; 75mW/mm^2], $P_{anesthetized}$ = [8mW/mm^2; 60mW/mm^2]) and imaging power densities were kept constant if not lower ($P_{i,awake}$ = [0.28mW/mm^2; 0.5mW/mm^2], $P_{i,anesthetized}$ = 0.5mW/mm^2). One plausible explanation for this spontaneous activity is increased activity of inhibitory neurons in the absence of anesthetics (Haider et al., 2013).

DISCUSSION

Achievements

We describe a new fiberscope that allows all-optical control and monitoring of neuronal activity in freely behaving rodents with near-cellular resolution. This is achieved using holographic targeted photoactivation of ChR2 and functional fluorescence imaging of GCaMP5-G.

Excitation patterns for targeted photoactivation were created by CGH and focused onto the input surface of a flexible fiber-bundle. The bundle and associated micro-objective transmitted and imaged the excitation patterns into the mouse brain. User-defined excitation patterns within a circular field of view of 240μm in diameter could be created (Figure S1). By using a 5μm spot centered on a single soma, photoactivation with near-cellular resolution was routinely possible in anesthetized and freely behaving mice. More precisely, in anesthetized animals, we measured lateral and axial resolutions to be approximately 7 and 35 μm (HWHM), respectively.

CGH also allows simultaneous targeting of multiple neurons by placing photoactivation spots on the corresponding somata. For example, here, 5 cells were simultaneously targeted while keeping a near-cellular resolution (Figure 4B). The maximum number of targeted cells depends on the maximum available laser power, in our case 17mW, at the objective. When this power is distributed across the full field of view, this corresponds to a power density (>230mW/mm^2) more than sufficient to obtain reliable photostimulation (50-75mW/mm^2). Therefore, all neurons in the field of view could be photostimulated at once. We note however that photoactivation resolution decreases when increasing the number of targeted cells because out-of-focus light from an increased number of photoactivation spots will add up and can become sufficient to excite out-of-focus somata or – more importantly – cellular processes including dendrites.

Regarding time resolution (T_R), our photoactivation protocol consisted of a 9Hz train of 24X60ms pulses or a 20Hz train of 60X5ms pulses. Alternative methods have used shorter photoactivation protocols (Andrasfalvy et al., 2010; Begue et al., 2013; Packer et al., 2012; Papagiakoumou et al., 2010; Prakash et al., 2012; Rickgauer and Tank, 2009; Wilson et al., 2012), as short as 1ms in the case of single photon (1P) (Wilson et al., 2012) or 2 photon (2P) CGH (Begue et al., 2013), for targeted photoactivation of ChR2 with cellular or near-cellular resolution in cell cultures, brain slices, and in anesthetized rodents. In these studies, T_R was defined as the time needed to generate a single action potential. Here, we used calcium imaging with GCaMP5-G as the response readout, with T_R defined as the time necessary to evoke a measurable $\Delta F/F$ (here, $\Delta F/F>20\%$), which corresponds to evoking several APs. With a more sensitive readout (such as GCaMP6), a shorter T_R is possible.

One major advantage of CGH with respect to laser scanning approaches is the shorter T_R needed for targeting multiple neurons. For scanning approaches, T_R is given by $T_R=(t_R + t_s) \times N$ (Vaziri and Emiliani, 2012), where t_R is the residence time at a given position (also known as the dwell time), t_S the point to point scanning time and N the number of targeted cells. Increased efficiency in photostimulation might require scanning the laser beam within the cell soma(ta) (Rickgauer and Tank, 2009), in this case N will correspond to the number of positions visited within each cell multiplied by the number of targeted cells. For CGH, the temporal resolution is given by $T_R = t_R$ and is independent of the number of excited cells, demonstrated here by simultaneous photostimulation of 5 cells (Figure 4B) with the same T_R as for single cell stimulation. For sequential projection of different photostimulation patterns with CGH, the refresh rate R_e of the LC-SLM imposes an additional time delay of $1/ R_e$ = 5-17ms between two patterns, and T_R becomes equal to (t_R+1/R_e) (Vaziri and Emiliani, 2012).

Previous functional imaging techniques for freely behaving rodents are reviewed in (Kerr and Nimmerjahn, 2012). In mice, epifluorescence imaging used fiberscopes (Ferezou et al., 2006; Flusberg et al., 2008; Murayama and Larkum,

2009) or fiberless head-mounted miniature microscopes (Ghosh et al., 2011; Ziv et al., 2013). However, these methods did not give optical sectioning. 2P imaging allows optical sectioning and has been performed in freely behaving rats with lateral resolution of 0.9µm (Sawinski et al., 2009) by using a head-mounted laser-scanning 2P microscope. The weight of the device, however, has not yet permitted extending this approach to freely behaving mice. Here, we describe a versatile system, capable of switching between epifluorescence, structured illumination, and multipoint confocal imaging, the latter two modalities giving optical sectioning. Structured illumination provides an improved contrast (by a factor 6.6) that was helpful in designing illumination patterns for photoactivation and confocal imaging. Confocal imaging provides a sharper PSF, allowing functional imaging from selected somata with lateral and axial resolutions of 3.1 and 8.6µm FWHM, respectively (Figure 2F-G, Figure S2D-E and SUPPLEMENTAL RESULTS).

Achieving an all-optical control and readout of neural activity requires combining functional imaging and photostimulation. This has been achieved in brain slices and in anesthetized animals by combining imaging of Ca^{2+} sensitive probes or voltage-sensitive dye (VSD) with glutamate uncaging, either with 1P excitation (Anselmi et al., 2011; Vogt et al., 2011; Zahid et al., 2010) or 2P excitation (Bloodgood and Sabatini, 2007; Losonczy and Magee, 2006; Losonczy et al., 2008; Nikolenko et al., 2007; Noguchi et al., 2011), or by combining VSD imaging with 1P ChR2 photoactivation (Lim et al., 2012; Tsuda et al., 2013; Willadt et al., in press). All these approaches benefit from a reduced overlap between the absorption spectra of the functional reporter and the photosensitive actuator. By contrast, combination of Ca^{2+} imaging with ChR2 photostimulation is a significant challenge due to the large overlap between absorption spectra of ChR2 and the most commonly used Ca^{2+} reporters, which can result in illumination light inducing photostimulation. Due to the low efficiency of ChR2 activation under 2P laser-scanning stimulation (Rickgauer and Tank, 2009), this effect can be reduced if Ca^{2+} imaging is performed using 2P laser scanning microscopy as recently demonstrated by Wilson and colleagues in anesthetized

mice (Wilson et al., 2013). This approach requires the use of a 2P scanning head, which is suitable for use with rats but has not yet been demonstrated in freely moving, smaller, mice. Here we found conditions that allowed for the first time in a living rodent, combined use of 1P ChR2 photostimulation and 1P functional imaging of a genetically encoded calcium reporter (GECI, here GCaMP5G) at near cellular resolution. These conditions included performing imaging in confocal mode, by illuminating only the soma(ta) of interest with extremely low light power (~6.10^{-3}µW per soma), and collecting fluorescence signals with a sensitive sCMOS camera. Because an all-optical approach allows taking full advantage of contemporary optogenetic tools, we believe this novel fiberscope is a powerful tool to investigate neuronal networks. Moreover, the same strategy can be implemented in a conventional 1P optical microscope permitting extension of this approach to brain slices or *in vivo* applications at shallow depths.

Current limitations and technical outlook

Our current fiberscope uses 1P excitation for photaoctivation and imaging and therefore required using a brain region with a relatively sparse pattern of labeled cells in order to approach cellular resolution. The synthesis of opsins localized to the soma and/or axon hillock (Greenberg et al., 2011; Wu et al., 2013) would reduce the contribution coming from out-of-focus dendritic or axonal processes, thus permitting increasing the effective resolution of photostimulation. The implementation of a 2P fiberscope allowing for 2P-CGH and 2P scanning imaging (Gobel et al., 2004) would permit a true cellular resolution both for photostimulation and for imaging. It will also permit reducing ChR2 photostimulation during Ca^{2+} imaging as suggested by Wilson and colleagues (Wilson et al., 2013).

As for any 1P fluorescence microscope, the imaging depth of our fiberscope is limited to a few tens of microns (~60µm-100µm with custom designed objective (Ziv et al., 2013)). Implementing a 2P fiberscope would allow increasing the working distance to >200µm (Sawinski et al., 2009). Access to deeper structures

could also be obtained by inserting the micro-objective or a smaller GRIN-lens based objective into the brain (Dombeck et al., 2010; Flusberg et al., 2008; Ghosh et al., 2011). To further reduce the diameter of the implanted optical probe, our fiberscope could be implemented with low-diameter beveled bundles (Vincent et al., 2006). However, since no micro-objective would be used in this case, this would degrade lateral and axial resolution and requires that imaged/photoactivated cells be located close to the bundle surface (where they could be potentially damaged by the bundle).

New strategies for transmission of light patterns through optical fibers use single-core multimode fibers and looks extremely promising as approaches for in-depth patterned photostimulation. They are based on digital phase conjugation, and require calculating the appropriate wavefront that brings light into defined patterns at the output of the fiber (Bianchi et al., 2013; Cizmar and Dholakia, 2012; Papadopoulos et al., 2013). However, one drawback of these techniques is that they are very sensitive to fiber bending. In fact, although recent improvements have been made in this regard (Farahi et al., 2013), whether these methods can be used in freely behaving animals remains to be shown.

In order to investigate long-term neuronal network dynamics, our technique can be adapted to chronic experimentation, providing that the micro-objective is implanted at the brain surface or inside the brain, e.g. in (Ziv et al., 2013).

Although our fiberscope in its current implementation allowed photoactivation and imaging within one unique plane, access to different planes could be obtained by using a micro-objective of variable focal length to image the output of the fiber bundle inside the brain, e.g., by inserting a micromotor to displace one of the micro-objective lenses (Flusberg et al., 2008).

Another potential technical advancement would be the development of a non-ferromagnetic objective, which would permit the use of the fiberscope with fMRI.

Opto-fMRI is indeed a promising field (Lee et al., 2010; Schulz et al., 2012) and our fiberscope would dramatically improve resolution for photoactivation and calcium imaging compared to current state-of-the-art.

As optogenetic tools improve, the performance of our system will improve likewise. For example, since our fiberscope is compatible with multiple light sources both in the stimulation and in the imaging pathways, actuators and reporters with reduced spectral overlap could be used, such as red GECI (Akerboom et al., 2013; Zhao et al., 2011) and standard ChR2, or green GECI and red or blue shifted opsins (Klapoetke et al., 2014; Lin et al., 2013). Imaging power density, which we kept low in order not to photoactivate ChR2, could therefore be increased, enabling higher signal to noise ratios (allowing for shorter photostimulation protocols) and/or higher imaging speed. Alternatively, simultaneous stimulation and inhibition, or simultaneous multicolor imaging could be performed using two ospins or calcium indicators with separate activation/absorption spectra. ChR2 patterned photostimulation combined with VSD imaging to probe the response from large neuronal populations is also a very promising approach (Lim et al., 2012), particularly in view of recent progress in the development of voltage sensitive genetically encoded probes (Gong et al., 2014; St-Pierre et al., 2014). Our system will permit extending these investigations to awake freely behaving rodents.

An advantage of CGH is that it is not limited to binary patterns, as used here, but can also produce graded patterns, with variable intensity levels (Conti et al.). This feature is particularly suited when patterned photostimulation is combined with a P2A based bi-cistronic labeling strategy (Prakash et al., 2012). In this case, the fluorescence intensity from the reporter (YFP, EYFP, mCherry, etc...) used to visualize ChR2 positive cells is proportional to the density of channels. This property can be used for scaling the holographic stimulation so that more light is directed onto dim cells compared to highly fluorescent cells, thus achieving more uniform excitation conditions.

Applications

The understanding of neuronal network function has gained immensely from advances in fluorescence imaging methods, which in particular have enabled simultaneous recording from multiple neurons. However, such studies would benefit greatly if one had the ability to manipulate in real time the activity of defined sets of neurons, in freely behaving animals. For example, in the cerebellum, targeted photoactivation of stellate cells would help analyzing MLI network activity and its relationship to Purkinje cells activity (Ozden et al., 2012; Sullivan et al., 2005).

Similarly, in neocortex layer 1, studies investigating local interneuronal networks that play a major role cortical integration of sensory and motor information (Jiang et al., 2013; Pfeffer et al., 2013) would be aided with targeted photoactivation of interneurons and simultaneous fluorescence imaging.

In the hippocampus and parahippocampal region, selective excitation or inhibition of place cells or grid cells could be most useful in elucidating place and grid codes during orientation and navigation (Moser et al., 2014; Ziv et al., 2013). Introduced into the brainstem, the fiberscope could be used to characterize respiratory central pattern generator properties, similarly to what holographic photostimulation has allowed ex vivo (Kam et al., 2013).

In general, this light sculpting fiberscope represents an extremely powerful tool for precise photostimulation and functional recording of brain activity and will help elucidating how neural circuit dynamics regulate animal behavior.

EXPERIMENTAL PROCEDURE

In vivo optical setup (Figure 1A)

The *in vivo* optical setup includes a homemade microscope combining photoactivation with CGH and fast fluorescence imaging. The microscope was coupled to the sample with a 2-meter long fiber bundle attached to an imaging

micro-objective (Ultra Mini O probe, Maunakea Technologies, Paris, France). Illumination patterns (for photoactivation and imaging) were projected at the focal plane of the microscope objective, where the proximal end of the imaging bundle was positioned, transmitted through the bundle and imaged onto the sample with the micro-objective. Similarly, fluorescence from the sample was imaged onto the distal end of the fiber bundle, transmitted through the bundle, and reimaged on a sCMOS camera (Orca Flash 4.0, Hamamatsu) using the microscope objective and a tube lens. The fiber bundle had 30,000 individual fiber cores distributed in a 600µm diameter imaging area. Each fiber core transmits one intensity pixel of the illumination patterns (for photoactivation or imaging) and fluorescence images. The distance between centers of adjacent fiber cores (3.3 µm at the bundle, 1.3µm at the sample) limits the spatial resolution of the techniques. The micro-objective had an external diameter of 2.6mm, a magnification of 2.5 (yielding a field-of-view of 240µm diameter), a working distance of 60µm, and a numerical aperture of 0.8.

Animal Care

All experiments followed European Union and institutional guidelines for the care and use of laboratory animals (Council directive 86/609 EEC) and were approved by the Paris Descartes Ethics Committee for Animal Research with the registered number CEEA34.EV.118.12.

Stereotactic injections of viral vectors

The following adeno-associated virus vectors were injected in the most dorsal lobe (IV/V) of the cerebellar vermis: AAV2/1.hSynap.Flex.GCaMP5G(GCaMP3-T302L.R303P.D380Y).WPRE.SV40 and AAV2/1.CAGGS.flex.ChR2.tdTomato.SV40 (University of Pennsylvania School of Medicine, Vector Core).

In vivo experiments, freely behaving mice

Head-plate fixation. A custom-made head-plate (Figure S5A) was fixed 29 to 86 days post injection for GCaMP5-G/ChR2 mice, or at P62-P68 for Rainbow mice. Mice were anesthetized with isoflurane saturated with O_2, initially at 5%,

adjusted to the minimal amount preventing pain reflexes (3-5%). Mice were placed in a restraining frame (SG4N, Narishige), on a heating pad, with eye cream and opaque paper on the eyes. Buprenorphine (20µg/kg) was injected intraperitoneally. After shaving, the scalp was incised and the periosteum removed. The skull (parietal and interparietal plates) was cleaned and gently scrubbed with a delicate bone scraper and 3% H_2O_2 was applied with a cotton bud. Dental primer and adhesive (Optibond FL, Kerr) were applied. For GCaMP5-G/ChR2 mice, an epifluorescence stereo-microscope was used to detect the pre-injected fluorescent lobule through the skull and the head-plate was positioned on the skull lateral to the earlier injection site. For Rainbow mice, the head-plate was positioned on the skull above the cerebellar vermis, lobe IV/V. The head-plate was cemented with photopolymerizable Tetric Evoflow material (Ivoclar Vivadent). The skin was then closed with surgical glue (Vetbond), and an additional dose of buprenorphine (20µg/kg) was injected intraperitoneally.

Surgery and micro-objective fixation. Experiments were conducted 2 to 4 days after head-plate fixation. Mice were anesthetized with isoflurane saturated with O_2 and placed in a restraining frame (see above). Buprenorphine (20µg/kg) was injected intraperitoneally. A 2.7mm diameter craniotomy was performed using a trephine and a 26G needle to score the final second tablet. Meninges were kept intact in 6 mice (and accidentally slightly opened in 2 other mice) and kept moistened with HEPES buffered ACSF. The micro-objective was then placed just touching the brain surface. Agar in ACSF (2%) was used to fill any small spaces between the head-plate and objective. Two M2 screws held the micro-objective to its holder. The holder was then fixed to the head-plate with Tetric Evoflow photopolymerizable cement, before being filled with agar in ACSF (2%). An additional dose of buprenorphine (20µg/kg) was injected intraperitoneally.

Awake mice experiments. A cage (40x25x20cm^3) containing 2-3 food pellets was placed on a rotating tray. Mice were put in the cage at least one hour before anesthesia in order to habituate them to this environment. During the experiment, no constraints were applied to the mice, and they could move freely

in the cage. Initially, the tray was manually rotated to avoid coiling of the fiber bundle and importing any torque. In our last experiments, however, we found that the mice did not significantly torque the fiber, so we could let them behave freely without rotating the cage. A CCD camera with red LED illumination was used to film the mouse during the experiment.

Author contributions:

V.S. developed methods for surgery and fixation of micro-objective on mice brain and performed AAV injections. C.V. designed and built the optical setup and developed the acquisition software. V.S. and C.V performed experiments and analysed data. J.B. designed the protocol for viral expression and performed the experiments in Rainbow PV-cre mice with C.V. V.dS. and V.E designed and wrote the software Wave front designer. C.V., and V.E. conceived the project and wrote the manuscript. V.S. and J.B. contributed to the writing. V.E. supervised the project.

Acknowledgement:

We thank MaunaKea Technologies for providing the fiberscope probe, and Jack Feldman for useful insights and proofreading the manuscript. We also thank Declan Lyons, Françoise Levavasseur, Elke Schmidt, Nicole Ropert and all others members of U603, as well as Pepe Alcami, Isabelle Llano, Clément Léna and Philippe Ascher for useful discussion, and insightful and constructive advice, and Isabel Llano and Jean Livet for the PV-Cre and Rainbow mice, respectively. We thank Dan Oron for the simulation of light propagation in scattering media. We also thank Abdelali Jalil for help with histology, Christophe Tourain and Patrice Jegouzo for technical assistance. We acknowledge the animal facility of Paris Descartes University. V.S. was supported by the Liliane Bettencourt Inserm School, the Frontiers in Life Sciences "FDV" PhD program and the Bettencourt-Schueller Foundation. This work was supported by C'Nano Ile de France, the Human Frontier Science Program (RGP0013/2010). We acknowledge Scott Sternson from Janelia Farm Institute for providing the AAV-FLEX-rev-ChR2-

tdtomato construct, and the Janelia Farm program for providing the GCaMP5-G construct, specifically Loren L. Looger, Jasper Akerboom, Douglas S. Kim and the Genetically Encoded Calcium Indicator (GECI) Project at Janelia Farm Research Campus Howard Hughes Medical Institute. We thank Maisie Lo and Karl Deisseroth from the Optogenetics Innovation Laboratory (OIL) for their workshop (http://biox.stanford.edu/biox/optogenetics_courses.html).

Figures

Figure 1: Optical setup of fiberscope and characterization of computer-generated holography (CGH).

A. Fiberscope is composed of two illumination paths: one for photoactivation with CGH (blue path) including a liquid-crystal spatial light modulator (LC-SLM), and a second for fluorescence imaging (dark green path) including a digital micromirror device (DMD). Backward fluorescence (light green path) was detected on a sCMOS camera. Paths were coupled to sample using a fiber bundle attached to a micro-objective (MO). L: lens (focal lengths are given in Figure S1A); BS: beamsplitter; O: microscope objective; F: emission filter.

B-E. Characterization of CGH. B. "Happy Face" illumination pattern generated with CGH and recorded with fiberscope from layer of (fluorescent) rhodamine, showing full field-of-view (diameter 240µm) that was accessible for photoactivation. C. Sections of photoactivation beam along the (x-y) plane (top) and (y-z) plane (bottom) for a 5µm diameter spot. D. Axial profile of beam shown in (B). Axial resolution, defined as the FWHM of this axial profile, was 18µm, in agreement with theoretical predictions (Figure S4A). E. Axial resolution (Δz_{FWHM}) of photoactivation beam as a function of spot diameter, *D*. Circles: experimental data. Solid line: linear fit of equation $\Delta z_{FWHM}=3D$.

See EXPERIMENTAL PROCEDURES and SUPPLEMENTAL EXPERIMENTAL PROCEDURES for details.

Figure 2: Characterization of fluorescence imaging with intensity modulation.

A. Implementation of epifluorescence and structured illumination microscopy (SIM). Optical layout corresponds to the imaging pathway of fiberscope setup (Figure 1A). Illumination mask displayed by the DMD is a uniform pattern for epifluorescence imaging (left), and a monodimensional grid pattern for SIM (right).

B-C. Characterization of epifluorescence and SIM imaging. B. Fluorescence images recorded in anesthetized mouse expressing GCAMP5-G in cerebellar interneurons following stereotaxic injection of Cre recombinase-dependent adeno-associated viruses (Figure S2A) with conventional epifluorescence imaging (left) and SIM (right). SIM allowed better background rejection, corresponding to a contrast increase by a factor 6.6 (n=10 cells). SIM was performed with a 43µm grid period; image processing included wavelet prefiltering. Exposure time was 40ms for epifluorescence and 3x40ms for SIM. C. Left. SIM intensity measured with fiberscope from a fluorescence plane as a function of axial position z (z=0 at imaging plane of micro-objective), for grid period 43µm, with (blue triangles) or without (black squares) wavelet prefiltering. Axial resolution, defined as FWHM of this optical sectioning curve, was 33 µm or 34 µm respectively. Right. Axial resolution of SIM as a function of grid period. Circles: experimental data. Solid line: linear fit.

See SUPPLEMENTAL EXPERIMENTAL PROCEDURES and Figure S2B-C for additional details on SIM.

D. Implementation of scanless multipoint confocal microscope for fluorescence recording from a few somata (in this case, 3). Illumination mask displayed by DMD acts as 3 virtual illumination pinholes, matching positions of 3 neurons in sample. On sCMOS camera, 3 corresponding ROIs were drawn (green circles), acting as virtual detection pinholes. For each neuron, fluorescence signal was integrated in corresponding ROI.

E. Left: Average of 600 raw images registered at camera in multipoint confocal mode, for simultaneous functional imaging of 3 somata. Right: GCaMP5-G calcium signal (ΔF/F trace) measured from 4.2µm ROI circled in green, and placed on soma. See Figure S6 for details. F. (x-z) profile of the confocal PSF. G. Lateral (left) and axial (right) profiles of the PSF: lateral and axial resolutions are 3.1µm and 8.6µm respectively (FWHM).

Figure 3: Combined photoactivation of ChR2 and imaging of GCaMP5-G in anesthetized mouse.

A. Protocol for functional imaging in mice co-expressing GCaMP5-G and ChR2. ΔF/F traces measured from a 4µm region of interest (ROI) placed on a cell body, for various configurations and power densities (Pi) of the imaging illumination beam. Curve 1: widefield uniform illumination, Pi= 0.5mW/mm^2; curves 2-6: illumination of the 4µm ROI only (scanless confocal configuration), Pi= 3mW/mm^2; 2mW/mm^2; 1.5mW/mm^2; 1mW/mm^2; 0.5mW/mm^2 respectively. The green horizontal bar represents illumination with imaging laser beam. In this experiment, the photoactivation laser was off. In widefield configuration a dramatic increase of the fluorescence signal was observed after imaging onset. This was interpreted as a result of widefield photoactivation with imaging light. Keeping the same imaging power density and limiting illumination to one soma with a 4µm diameter spot (scanless confocal configuration) gave a stable baseline (curve 6). We interpreted this as unaffected neuron baseline activity. For Pi ≥ 1mW/mm^2, a small increase of the baseline was observed following imaging onset (curves 2-5). Therefore, functional imaging was performed in the confocal configuration with Pi≤ 0.5mW/mm^2. Widefield ΔF/F trace is single trial. Other ΔF/F traces were obtained by averaging 2 trials (curve 2, 3, 5), 3 trials (curve 4) or 5 trials (curve 6).

B-C. Photoactivation of ChR2 in anesthetized mice.

B. Bottom. Photoactivation protocol (blue line, Ph) was a 9Hz train of light pulses (24 pulses of 60ms duration) of 5µm diameter CGH spots. Imaging was performed in the multipoint confocal configuration, under continuous illumination (green line, Im) with a power density Pi=0.5mW/mm^2. Exposure time was 40 ms. Acquisition rate was 18-20Hz before and after photoactivation, and lowered to 9Hz during photoactivation because imaging was only performed between the photoactivation pulses (black line, Acq, represents successive camera exposures). Top trace. Single cell somatic calcium signal triggered by photoactivation between t=0 and t=t_p. Red, fit with a piecewise-defined function (linear rising phase and monoexponential decay; τ=0.96s). Calcium signal amplitude ($\Delta F/F_P$) was defined as fit function amplitude at t_p. Here, $\Delta F/F_P$=

107%. Power density of the photoactivation beam: P=25mW/mm^2. Bottom trace. The same experiment was repeated in a control mouse expressing GCaMP5-G only. P=75mW/mm^2.

C. Repeating the photoactivation protocol reliably triggered calcium signals over 12 trials in same neuron. P=25mW/mm^2. Trace was low-pass filtered with a moving 5-point average filter.

Signal traces shown in B-C are single trial.

Figure 4: Characterization of photoactivation lateral and axial selectivity in anesthetized mice.

Unless stated otherwise, photoactivation and imaging protocols are the same as in Figure 3.

A. Left. Inset: geometry of a MLI (schematized in green) with axes x, y and z used to characterized photoactivation selectivity. x-axis represents horizontal axis perpendicular to sagittal plane containing dendrites. y- and z-axes represent horizontal and vertical axes in sagittal plane containing dendrites. Main figure: Ratio (R) of $\Delta F/F_P$ obtained for a photoactivation spot placed off-cell versus on-cell, as a function of distance between spot and soma center along the x axis. For each neuron, first and last measurements were performed with photoactivation spot on-cell. $\Delta F/F_P$ were normalized to first measurement. Grey squares: data from n=14 cells from 7 mice. Blue squares: mean of all data. Error bars represent 95% confidence intervals of mean (CI95). P=8-50mW/mm^2 depending on neuron.

Middle. Ratio R obtained when photoactivation spot was displaced above the cell along z axis in 10µm steps. For each cell, the last measurement was performed with a photoactivation spot on cell, and calcium signal amplitudes $\Delta F/F_p$ were normalized to this measurement. Grey circles: data from n=3 cells from 1 mouse. Photoactivation protocol consisted in a unique pulse of 1s duration. Red circles: mean of all data. Error bars represent CI95. P=50mW/mm^2.

Right. Ratio R of $\Delta F/F_P$ measured when photoactivation spot placed off-cell versus on-cell, as a function of the distance between the spot and soma center in three directions: x (blue squares), y (black triangles) and z (red circles). Results for x and z axes are similar to shown in left and middle panels. Results for y axis are also shown in Figure S4B, and represent mean of data from n=4 cells from 1 mouse (P=40-60mW/mm^2 depending on neuron). Solid lines represent expected resolution in absence of scattering and assuming that only soma was labeled, in lateral (x, y, blue line) and axial (z, red line) directions. This expected resolution was calculated as the convolution between the measured 3D intensity profile of the 5µm diameter spots used for photostimulation (Figure 1C) and a sphere of diameter 7µm representing the soma membrane (see SUPPLEMENTAL EXPERIMENTAL PROCEDURES for details).

B. Simultaneous targeting of multiple cells. Top. SIM images. Blue disks indicate positions of photoactivation spots (but are larger than actual spot size for figure readability). Grid period: 43µm. Exposure time: 3x40ms. x and y axes are as defined in inset of figure A, left. Bottom. Corresponding ΔF/F traces registered simultaneously in 5 cells, numbered 1-5 and located in different parasagittal planes. Left: only cell #1 was targeted. Center: 5 cells were simultaneously targeted. Right: Photoactivation spot that targeted cell #1 displaced 20µm in coronal plane, as indicated by the white arrow. P=30mW/mm^2.

Figure 5: Fluorescence imaging and characterization of movements between the fiberscopic probe and the brain in freely behaving mice.

A. Picture of unrestrained (freely behaving) mouse in its cage with fiberscopic probe fixed to skull.

B SIM image recorded in freely behaving mouse co-expressing GCaMP5-G and ChR2 in MLIs, and showing MLI somata. Inset: single MLI with portion of dendrite (arrow). Grid period: 43µm. Exposure time: 3x200ms.

C. SIM image recorded in freely behaving Rainbow mouse expressing eYFP in

Purkinje cells, showing Purkinje cell dendritic tree segments. Grid period: 43µm. Exposure time: 3x200ms.

D-G. Quantification of movement between the fiberscopic probe and the brain. Lateral translation (x, blue squares and y, red triangles) and rotation (Θ green disks) are measured on different timescales: during 100s (D-E) and 200min (F-G).

D. Position of observed region of the brain along x and y monitored at 19Hz during 100s in 3 Rainbow mice (labeled #R1, #R2, #R3). Behavior of mouse indicated as background color; blue: body displacement; yellow: head movement; green: eating; grey: still. Lateral translations are multiple of the pixel size (0.47µm).

E. For each mouse, experiment shown in D was repeated 10 times, and maximum displacements Δx (blue squares) and Δy (red triangles) for each acquisition as indicated. Please note that several acquisitions gave the same amount of displacement. Averages of maximum movements along x and y over all 10 acquisitions are given by black squares and black triangles respectively, for each mouse. Error bars correspond to CI95.

F-G Translation and rotation of observed brain region monitored during 200min in 6 mice. Figure F shows positions of observed brain region as a function of time for 2 mice co-expressing GCaMP5 and ChR2 in MLIs. Data for all mice shown in Figure S5C. The maximum translation (Δx, blue squares; Δy, red triangles; left ordinate) and rotation (ΔΘ, green circles; right ordinate) for each mouse are plotted on Figure G. Average displacements over mice are given by black squares (Δx), triangles (Δy), and circles (ΔΘ). Error bars correspond to CI95.

Figure 6: Photoactivation with near-cellular resolution in freely behaving mice.

Single cell photoactivation and imaging with same protocol as Figure 2 in mice co-expressing ChR2 and GCaMP5-G in MLIs. Signal traces shown are single trial.

A. Single cell somatic calcium signal triggered by photoactivation (blue line)

(P=50mW/mm^2). Black trace, experimental data. Red line, fit with a piecewise-defined function (linear rising phase and monoexponential decay), corresponding to a calcium signal amplitude $\Delta F/F_P$ =129%.

B. Ratio R of $\Delta F/F_p$ obtained for a photoactivation spot placed off-cell versus on-cell, as a function of distance between spot and soma center along the x-axis (as defined in inset of figure 4A, left). For each cell, last measurement was performed with a photoactivation spot on cell, and calcium signal amplitudes $\Delta F/F_p$ were normalized to this measurement. Grey squares: data from n=18 cells from 5 mice. Blue squares: mean of all data. Error bars represent CI95. P=25-75mW/mm^2.

C. (Top) Same photoactivation protocol (blue lines) as in A repeated every 30s for 15min (P=50mW/mm^2, Pi=0.28mW/mm^2). Trace was low-pass filtered with a moving 5-point average filter. (Bottom) Blowup of top trace showing spontaneous activity that occurred between evoked transients. Decay time of spontaneous calcium transients is similar to that of photoactivation-triggered transients.

References

Akerboom, J., Carreras Calderon, N., Tian, L., Wabnig, S., Prigge, M., Tolo, J., Gordus, A., Orger, M.B., Severi, K.E., Macklin, J.J.*, et al.* (2013). Genetically encoded calcium indicators for multi-color neural activity imaging and combination with optogenetics. Frontiers in molecular neuroscience *6*, 2-2.

Akerboom, J., Chen, T.W., Wardill, T.J., Tian, L., Marvin, J.S., Mutlu, S., Calderón, N.C., Esposti, F., Borghuis, B.G., Sun, X.R.*, et al.* (2012). Optimization of a GCaMP calcium indicator for neural activity imaging. J Neurosci *32*, 13819-13840.

Andrasfalvy, B.K., Zemelman, B.V., Tang, J., and Vaziri, A. (2010). Two-photon single-cell optogenetic control of neuronal activity by sculpted light. Proc Natl Acad Sci U S A *107*, 11981-11986.

Anselmi, F., Ventalon, C., Begue, A., Ogden, D., and Emiliani, V. (2011). Three-dimensional imaging and photostimulation by remote-focusing and holographic light patterning. Proc Natl Acad Sci U S A *108*, 19504-19509.

Aravanis, A.M., Wang, L.P., Zhang, F., Meltzer, L.A., Mogri, M.Z., Schneider, M.B., and Deisseroth, K. (2007). An optical neural interface: in vivo control of rodent

motor cortex with integrated fiberoptic and optogenetic technology. Journal of Neural Engineering *4*, S143-S156.

Barski, J.J., Dethleffsen, K., and Meyer, M. (2000). Cre recombinase expression in cerebellar Purkinje cells. Genesis *28*, 93-98.

Begue, A., Papagiakoumou, E., Leshem, B., Conti, R., Enke, L., Oron, D., and Emiliani, V. (2013). Two-photon excitation in scattering media by spatiotemporally shaped beams and their application in optogenetic stimulation. Biomedical Optics Express *4*, 2869-2879.

Bianchi, S., Rajamanickam, V.P., Ferrara, L., Di Fabrizio, E., Liberale, C., and Di Leonardo, R. (2013). Focusing and imaging with increased numerical apertures through multimode fibers with micro-fabricated optics. Optics Letters *38*, 4935-4938.

Bloodgood, B.L., and Sabatini, B.L. (2007). Nonlinear regulation of unitary synaptic signals by CaV(2.3) voltage-sensitive calcium channels located in dendritic spines. Neuron *53*, 249-260.

Bozinovic, N., Ventalon, C., Ford, T., and Mertz, J. (2008). Fluorescence endomicroscopy with structured illumination. Optics Express *16*, 8016-8025.

Cizmar, T., and Dholakia, K. (2012). Exploiting multimode waveguides for pure fibre-based imaging. Nature Communications *3*.

Conti, R., Assayag, O., DeSars, V., and Emiliani, V. in preparation.

Deisseroth, K. (2011). Optogenetics. Nature Methods *8*, 26-29.

Dhawale, A.K., Hagiwara, A., Bhalla, U.S., Murthy, V.N., and Albeanu, D.F. (2010). Non-redundant odor coding by sister mitral cells revealed by light addressable glomeruli in the mouse. Nat Neurosci *13*, 1404-1412.

Dombeck, D.A., Harvey, C.D., Tian, L., Looger, L.L., and Tank, D.W. (2010). Functional imaging of hippocampal place cells at cellular resolution during virtual navigation. Nat Neurosci *13*, 1433-1440.

Farahi, S., Ziegler, D., Papadopoulos, I.N., Psaltis, D., and Moser, C. (2013). Dynamic bending compensation while focusing through a multimode fiber. Optics Express *21*, 22504-22514.

Ferezou, I., Bolea, S., and Petersen, C.C.H. (2006). Visualizing the cortical representation of whisker touch: Voltage-sensitive dye imaging in freely moving mice. Neuron *50*, 617-629.

Flusberg, B.A., Nimmerjahn, A., Cocker, E.D., Mukamel, E.A., Barretto, R.P.J., Ko, T.H., Burns, L.D., Jung, J.C., and Schnitzer, M.J. (2008). High-speed, miniaturized fluorescence microscopy in freely moving mice. Nature Methods *5*, 935-938.

Franconville, R., Revet, G., Astorga, G., Schwaller, B., and Llano, I. (2011). Somatic calcium level reports integrated spiking activity of cerebellar interneurons in vitro and in vivo. Journal of Neurophysiology *106*, 1793-1805.

Ghosh, K.K., Burns, L.D., Cocker, E.D., Nimmerjahn, A., Ziv, Y., El Gamal, A., and Schnitzer, M.J. (2011). Miniaturized integration of a fluorescence microscope. Nature Methods *8*, 871-U147.

Gobel, W., Kerr, J.N.D., Nimmerjahn, A., and Helmchen, F. (2004). Miniaturized two-photon microscope based on a flexible coherent fiber bundle and a gradient-index lens objective. Optics Letters *29*, 2521-2523.

Gong, Y., Wagner, M.J., Zhong Li, J., and Schnitzer, M.J. (2014). Imaging neural spiking in brain tissue using FRET-opsin protein voltage sensors. Nat Commun *5*, 3674.

Greenberg, K.P., Pham, A., and Werblin, F.S. (2011). Differential Targeting of Optical Neuromodulators to Ganglion Cell Soma and Dendrites Allows Dynamic Control of Center-Surround Antagonism. Neuron *69*, 713-720.

Haider, B., Haeusser, M., and Carandini, M. (2013). Inhibition dominates sensory responses in the awake cortex. Nature *493*, 97-+.

Hayashi, Y., Tagawa, Y., Yawata, S., Nakanishi, S., and Funabiki, K. (2012). Spatio-temporal control of neural activity in vivo using fluorescence microendoscopy. European Journal of Neuroscience *36*, 2722-2732.

Huber, D., Petreanu, L., Ghitani, N., Ranade, S., Hromadka, T., Mainen, Z., and Svoboda, K. (2008). Sparse optical microstimulation in barrel cortex drives learned behaviour in freely moving mice. Nature *451*, 61-U67.

Jiang, X., Wang, G., Lee, A.J., Stornetta, R.L., and Zhu, J.J. (2013). The organization of two new cortical interneuronal circuits. Nature Neuroscience *16*, 210-218.

Kam, K., Worrell, J.W., Ventalon, C., Emiliani, V., and Feldman, J.L. (2013). Emergence of Population Bursts from Simultaneous Activation of Small Subsets of preBotzinger Complex Inspiratory Neurons. Journal of Neuroscience *33*, 3332-3338.

Kerr, J.N., and Nimmerjahn, A. (2012). Functional imaging in freely moving animals. Curr Opin Neurobiol *22*, 45-53.

Kim, J., Lee, S., Tsuda, S., Zhang, X.Y., Asrican, B., Gloss, B., Feng, G.P., and Augustine, G.J. (2014). Optogenetic Mapping of Cerebellar Inhibitory Circuitry

Reveals Spatially Biased Coordination of Interneurons via Electrical Synapses. Cell Reports *7*, 1601-1613.

Kim, T.I., McCall, J.G., Jung, Y.H., Huang, X., Siuda, E.R., Li, Y.H., Song, J.Z., Song, Y.M., Pao, H.A., Kim, R.H.*, et al.* (2013). Injectable, Cellular-Scale Optoelectronics with Applications for Wireless Optogenetics. Science *340*, 211-216.

Kitamura, T., Pignatelli, M., Suh, J., Kohara, K., Yoshiki, A., Abe, K., and Tonegawa, S. (2014). Island Cells Control Temporal Association Memory. Science *343*, 896-901.

Klapoetke, N.C., Murata, Y., Kim, S.S., Pulver, S.R., Birdsey-Benson, A., Cho, Y.K., Morimoto, T.K., Chuong, A.S., Carpenter, E.J., Tian, Z.*, et al.* (2014). Independent optical excitation of distinct neural populations. Nat Meth *11*, 338-346.

LeChasseur, Y., Dufour, S., Lavertu, G., Bories, C., Deschenes, M., Vallee, R., and De Koninck, Y. (2011). A microprobe for parallel optical and electrical recordings from single neurons in vivo. Nature Methods *8*, 319-U363.

Lee, J.H., Durand, R., Gradinaru, V., Zhang, F., Goshen, I., Kim, D.S., Fenno, L.E., Ramakrishnan, C., and Deisseroth, K. (2010). Global and local fMRI signals driven by neurons defined optogenetically by type and wiring. Nature *465*, 788-792.

Lim, D.H., Mohajerani, M.H., Ledue, J., Boyd, J., Chen, S., and Murphy, T.H. (2012). In vivo Large-Scale Cortical Mapping Using Channelrhodopsin-2 Stimulation in Transgenic Mice Reveals Asymmetric and Reciprocal Relationships between Cortical Areas. Front Neural Circuits *6*, 11.

Lin, J.Y., Knutsen, P.M., Muller, A., Kleinfeld, D., and Tsien, R.Y. (2013). ReaChR: a red-shifted variant of channelrhodopsin enables deep transcranial optogenetic excitation. Nature Neuroscience *16*, 1499-+.

Losonczy, A., and Magee, J.C. (2006). Integrative properties of radial oblique dendrites in hippocampal CA1 pyramidal neurons. Neuron *50*, 291-307.

Losonczy, A., Makara, J.K., and Magee, J.C. (2008). Compartmentalized dendritic plasticity and input feature storage in neurons. Nature *452*, 436-441.

Lutz, C., Otis, T.S., DeSars, V., Charpak, S., DiGregorio, D.A., and Emiliani, V. (2008). Holographic photolysis of caged neurotransmitters. Nature Methods *5*, 821-827.

Madisen, L., Mao, T.Y., Koch, H., Zhuo, J.M., Berenyi, A., Fujisawa, S., Hsu, Y.W.A., Garcia, A.J., Gu, X., Zanella, S.*, et al.* (2012). A toolbox of Cre-dependent optogenetic transgenic mice for light-induced activation and silencing. Nature Neuroscience *15*, 793-802.

Miesenboeck, G. (2011). Optogenetic Control of Cells and Circuits. Annual Review of Cell and Developmental Biology, Vol 27 *27*, 731-758.

Moser, E.I., Roudi, Y., Witter, M.P., Kentros, C., Bonhoeffer, T., and Moser, M.B. (2014). Grid cells and cortical representation. Nature Reviews Neuroscience *15*, 466-481.

Murayama, M., and Larkum, M.E. (2009). In vivo dendritic calcium imaging with a fiberoptic periscope system. Nature Protocols *4*, 1551-1559.

Nagel, G., Szellas, T., Huhn, W., Kateriya, S., Adeishvili, N., Berthold, P., Ollig, D., Hegemann, P., and Bamberg, E. (2003). Channelrhodopsin-2, a directly light-gated cation-selective membrane channel. Proceedings of the National Academy of Sciences of the United States of America *100*, 13940-13945.

Neil, M.A.A., Juskaitis, R., and Wilson, T. (1997). Method of obtaining optical sectioning by using structured light in a conventional microscope. Optics Letters *22*, 1905-1907.

Nikolenko, V., Poskanzer, K.E., and Yuste, R. (2007). Two-photon photostimulation and imaging of neural circuits. Nat Methods *4*, 943-950.

Noguchi, J., Nagaoka, A., Watanabe, S., Ellis-Davies, G.C., Kitamura, K., Kano, M., Matsuzaki, M., and Kasai, H. (2011). In vivo two-photon uncaging of glutamate revealing the structure-function relationships of dendritic spines in the neocortex of adult mice. J Physiol *589*, 2447-2457.

Ozden, I., Dombeck, D.A., Hoogland, T.M., Tank, D.W., and Wang, S.S.H. (2012). Widespread State-Dependent Shifts in Cerebellar Activity in Locomoting Mice. Plos One *7*, 16.

Packer, A.M., Peterka, D.S., Hirtz, J.J., Prakash, R., Deisseroth, K., and Yuste, R. (2012). Two-photon optogenetics of dendritic spines and neural circuits. Nature Methods *9*, 1202-U1103.

Papadopoulos, I.N., Farahi, S., Moser, C., and Psaltis, D. (2013). High-resolution, lensless endoscope based on digital scanning through a multimode optical fiber. Biomedical Optics Express *4*, 260-270.

Papagiakoumou, E., Anselmi, F., Begue, A., de Sars, V., Gluckstad, J., Isacoff, E.Y., and Emiliani, V. (2010). Scanless two-photon excitation of channelrhodopsin-2. Nature Methods *7*, 848-U117.

Petreanu, L., Huber, D., Sobczyk, A., and Svoboda, K. (2007). Channelrhodopsin-2-assisted circuit mapping of long-range callosal projections. Nat Neurosci *10*, 663-668.

Pfeffer, C.K., Xue, M.S., He, M., Huang, Z.J., and Scanziani, M. (2013). Inhibition of inhibition in visual cortex: the logic of connections between molecularly distinct interneurons. Nature Neuroscience *16*, 1068-U1130.

Pisanello, F., Sileo, L., Oldenburg, I.A., Pisanello, M., Martiradonna, L., Assad, J.A., Sabatini, B.L., and De Vittorio, M. (2014). Multipoint-Emitting Optical Fibers for Spatially Addressable In Vivo Optogenetics. Neuron *82*, 1245-1254.

Prakash, R., Yizhar, O., Grewe, B., Ramakrishnan, C., Wang, N., Goshen, I., Packer, A.M., Peterka, D.S., Yuste, R., Schnitzer, M.J.*, et al.* (2012). Two-photon optogenetic toolbox for fast inhibition, excitation and bistable modulation. Nature Methods *9*, 1171-U1132.

Rickgauer, J.P., and Tank, D.W. (2009). Two-photon excitation of channelrhodopsin-2 at saturation. Proc Natl Acad Sci U S A *106*, 15025-15030.

Rieubland, S., Roth, A., and Hausser, M. (2014). Structured Connectivity in Cerebellar Inhibitory Networks. Neuron *81*, 913-929.

Royer, S., Zemelman, B.V., Barbic, M., Losonczy, A., Buzsaki, G., and Magee, J.C. (2010). Multi-array silicon probes with integrated optical fibers: light-assisted perturbation and recording of local neural circuits in the behaving animal. European Journal of Neuroscience *31*, 2279-2291.

Sawinski, J., Wallace, D.J., Greenberg, D.S., Grossmann, S., Denk, W., and Kerr, J.N.D. (2009). Visually evoked activity in cortical cells imaged in freely moving animals. Proceedings of the National Academy of Sciences of the United States of America *106*, 19557-19562.

Schulz, K., Sydekum, E., Krueppel, R., Engelbrecht, C.J., Schlegel, F., Schroeter, A., Rudin, M., and Helmchen, F. (2012). Simultaneous BOLD fMRI and fiber-optic calcium recording in rat neocortex. Nature Methods *9*, 597-+.

St-Pierre, F., Marshall, J.D., Yang, Y., Gong, Y., Schnitzer, M.J., and Lin, M.Z. (2014). High-fidelity optical reporting of neuronal electrical activity with an ultrafast fluorescent voltage sensor. Nat Neurosci *17*, 884-889.

Stark, E., Koos, T., and Buzsaki, G. (2012). Diode probes for spatiotemporal optical control of multiple neurons in freely moving animals. Journal of Neurophysiology *108*, 349-363.

Sullivan, M.R., Nimmerjahn, A., Sarkisov, D.V., Helmchen, F., and Wang, S.S. (2005). In vivo calcium imaging of circuit activity in cerebellar cortex. Journal of neurophysiology *94*, 1636-1644.

Tabansky, I., Lenarcic, A., Draft, R.W., Loulier, K., Keskin, D.B., Rosains, J., Rivera-Feliciano, J., Lichtman, J.W., Livet, J., Stern, J.N.H.*, et al.* (2013). Developmental Bias in Cleavage-Stage Mouse Blastomeres. Current Biology *23*, 21-31.

Tsuda, S., Kee, M.Z., Cunha, C., Kim, J., Yan, P., Loew, L.M., and Augustine, G.J. (2013). Probing the function of neuronal populations: combining micromirror-

based optogenetic photostimulation with voltage-sensitive dye imaging. Neurosci Res *75*, 76-81.

Vaziri, A., and Emiliani, V. (2012). Reshaping the optical dimension in optogenetics. Curr Opin Neurobiol *22*, 128-137.

Vincent, P., Maskos, U., Charvet, I., Bourgeais, L., Stoppini, L., Leresche, N., Changeux, J.P., Lambert, R., Meda, P., and Paupardin-Tritsch, D. (2006). Live imaging of neural structure and function by fibred fluorescence microscopy. EMBO reports *7*, 1154-1161.

Vogt, K.E., Gerharz, S., Graham, J., and Canepari, M. (2011). Combining membrane potential imaging with L-glutamate or GABA photorelease. PLoS One *6*, e24911.

Willadt, S., Canepari, M., Yan, P., Loew, L.M., and Vogt, K.E. (in press). Combined Optogenetics and Voltage Sensitive Dye Imaging at Single Cell Resolution. Front in Cellular Neuroscience.

Wilson, N.R., Runyan, C.A., Wang, F.L., and Sur, M. (2012). Division and subtraction by distinct cortical inhibitory networks in vivo. Nature *488*, 343-348.

Wilson, N.R., Schummers, J., Runyan, C.A., Yan, S.X., Chen, R.E., Deng, Y.T., and Sur, M. (2013). Two-way communication with neural networks in vivo using focused light. Nature Protocols *8*, 1184-1203.

Wu, C.W., Ivanova, E., Zhang, Y., and Pan, Z.H. (2013). rAAV-Mediated Subcellular Targeting of Optogenetic Tools in Retinal Ganglion Cells In Vivo. Plos One *8*, 10.

Zahid, M., Velez-Fort, M., Papagiakoumou, E., Ventalon, C., Angulo, M.C., and Emiliani, V. (2010). Holographic Photolysis for Multiple Cell Stimulation in Mouse Hippocampal Slices. Plos One *5*.

Zhao, Y., Araki, S., Jiahui, W., Teramoto, T., Chang, Y.-F., Nakano, M., Abdelfattah, A.S., Fujiwara, M., Ishihara, T., Nagai, T.*, et al.* (2011). An Expanded Palette of Genetically Encoded Ca2+ Indicators. Science *333*, 1888-1891.

Ziv, Y., Burns, L.D., Cocker, E.D., Hamel, E.O., Ghosh, K.K., Kitch, L.J., El Gamal, A., and Schnitzer, M.J. (2013). Long-term dynamics of CA1 hippocampal place codes. Nature Neuroscience *16*, 264-266.

Zorzos, A.N., Scholvin, J., Boyden, E.S., and Fonstad, C.G. (2012). Three-dimensional multiwaveguide probe array for light delivery to distributed brain circuits. Optics Letters *37*, 4841-4843.

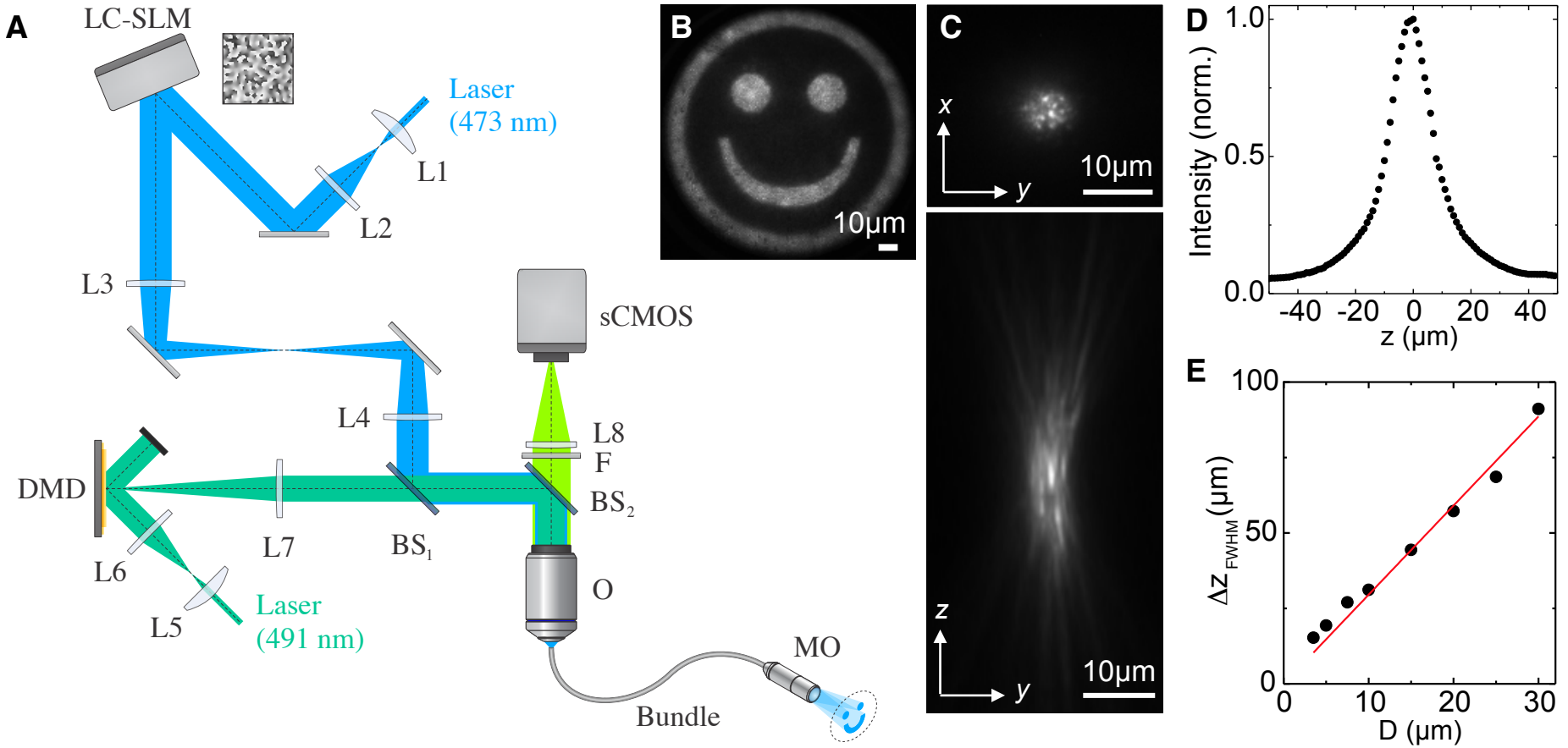
A
LC-SLM
Laser
(473 nm)
L1
L2
L3
sCMOS
L4
L8
F
DMD
BS2
L7
BS1
L6
O
L5
Laser
(491 nm)
MO
Bundle
B
10μm
C
x
y
10μm
z
y
10μm
D
Intensity (norm.)
1.0
0.5
0.0
-40 -20 0 20 40
z (μm)
E
100
50
0
0 10 20 30
D (μm)
ΔzFWHM (μm)

Figure 1

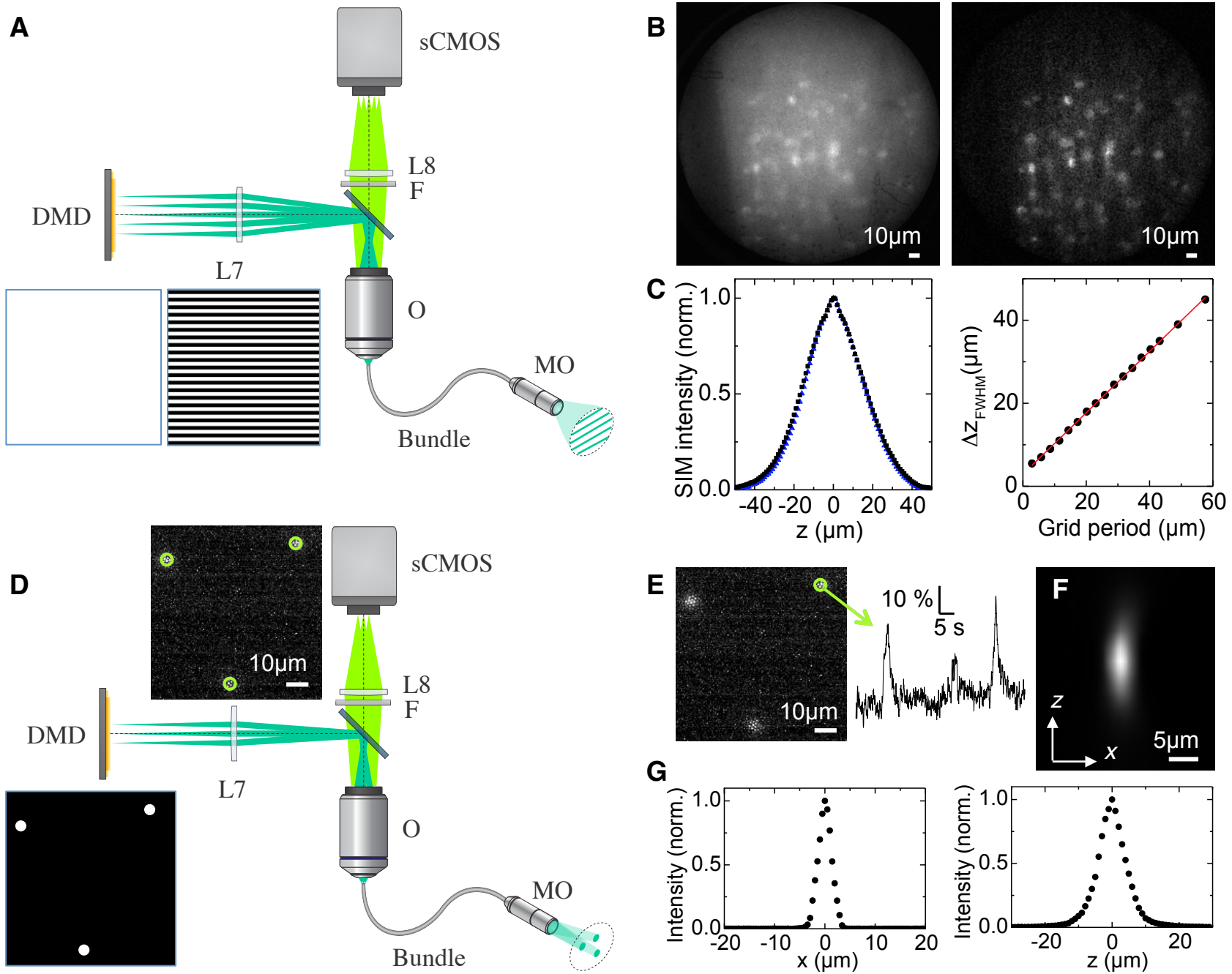
A
sCMOS
L8
F
DMD
L7
O
MO
Bundle
B
10μm
10μm
C
SIM intensity (norm.)
1.0
0.5
0.0
-40 -20 0 20 40
z (μm)
Δz_{FWHM} (μm)
40
20
0
0 20 40 60
Grid period (μm)
D
sCMOS
10μm
L8
F
DMD
L7
O
MO
Bundle
E
10μm
10 %
5 s
F
z
x
5μm
G
Intensity (norm.)
1.0
0.5
0.0
-20 -10 0 10 20
x (μm)
Intensity (norm.)
1.0
0.5
0.0
-20 0 20
z (μm)

Figure 2

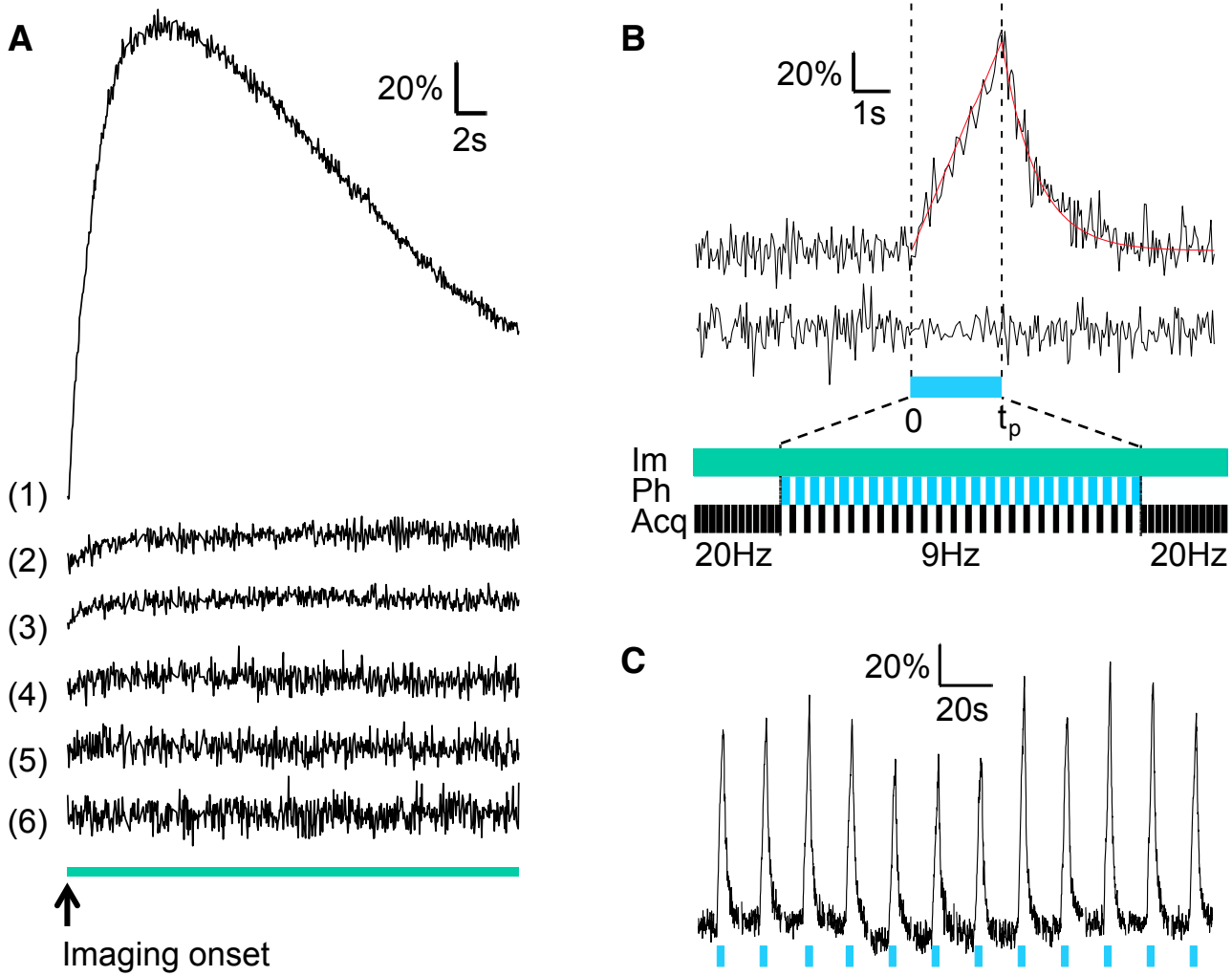
A
20%
2s
(1)
(2)
(3)
(4)
(5)
(6)
Imaging onset
B
20%
1s
0
t_p
Im
Ph
Acq
20Hz
9Hz
20Hz
C
20%
20s

Figure 3

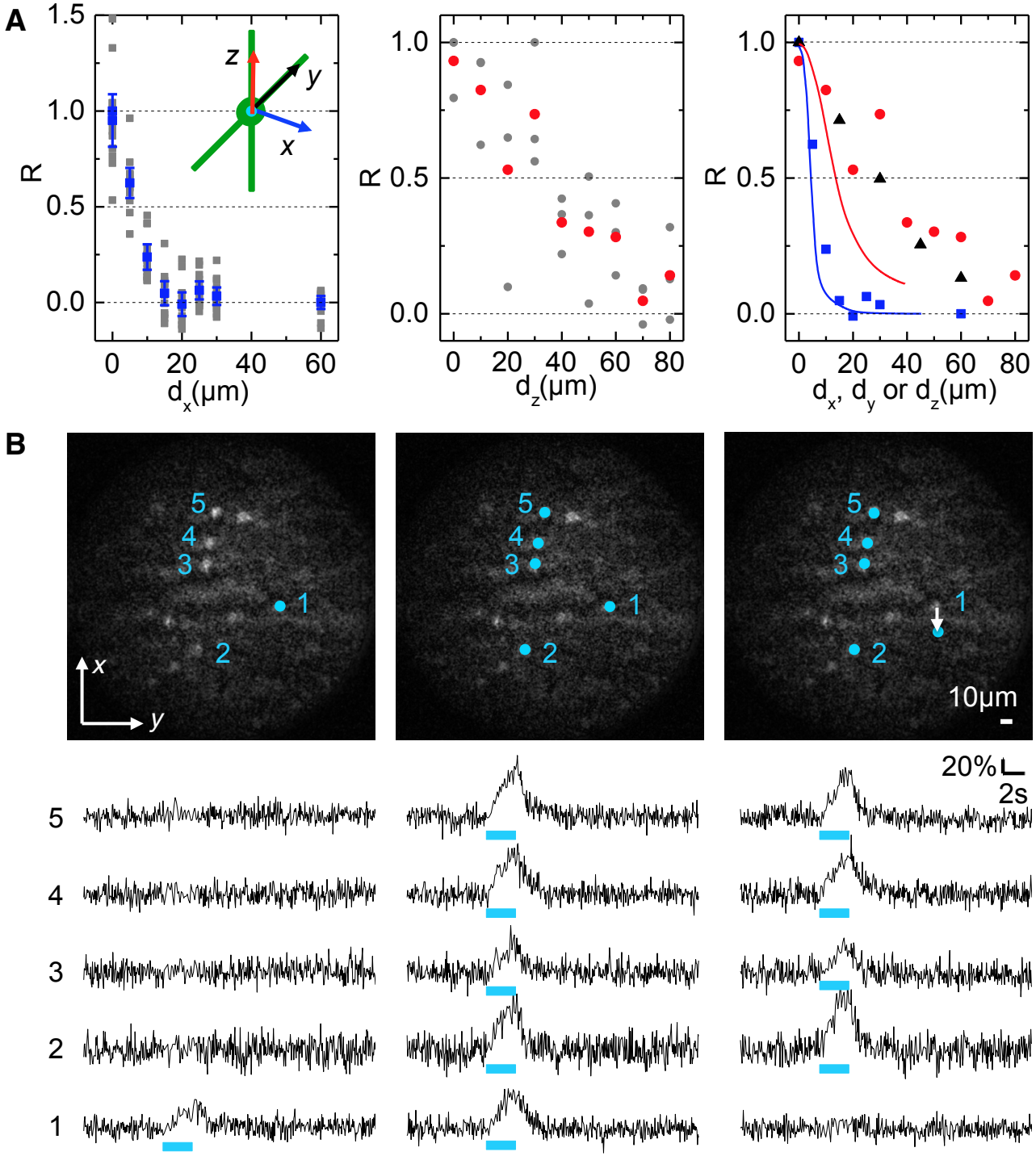

Figure 4

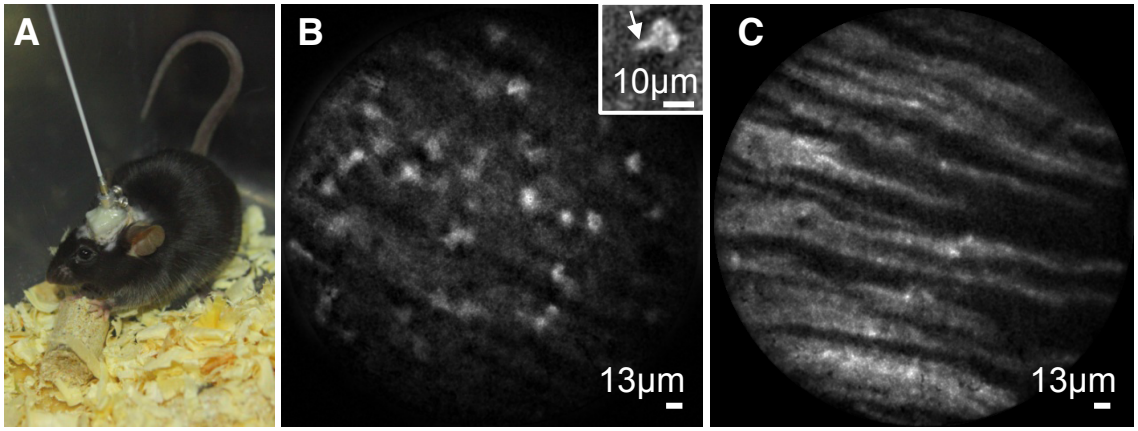
A
B
10μm
13μm
C
13μm

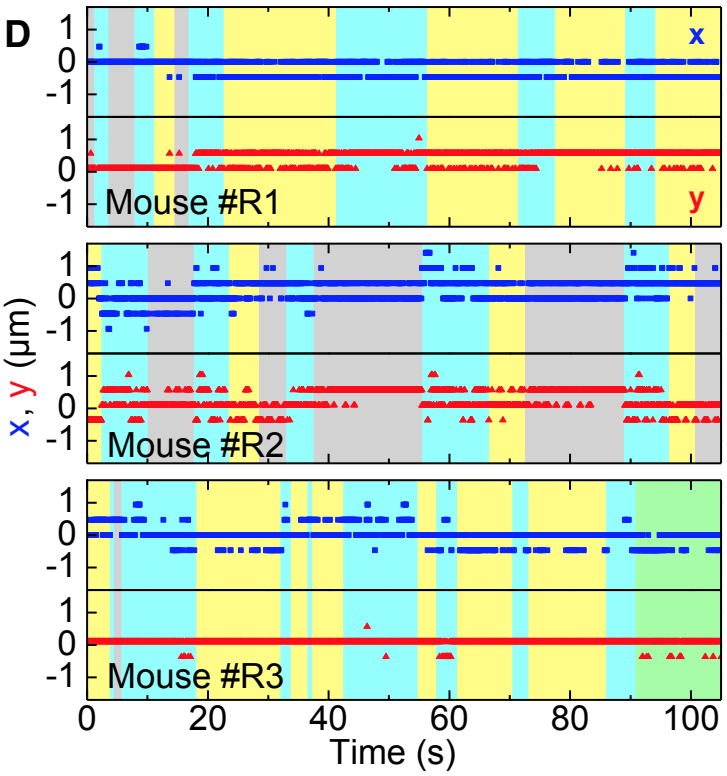
D
x
y
Mouse #R1
Mouse #R2
Mouse #R3
x, y (μm)
Time (s)

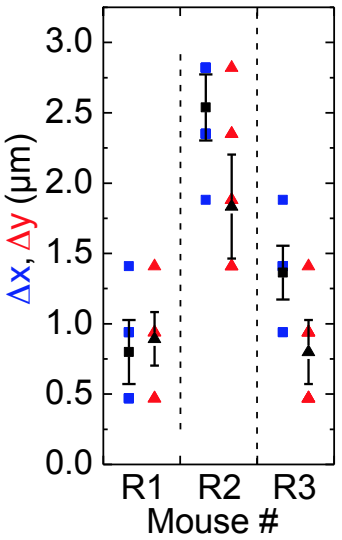
E
Δx, Δy (μm)
R1
R2
R3
Mouse #

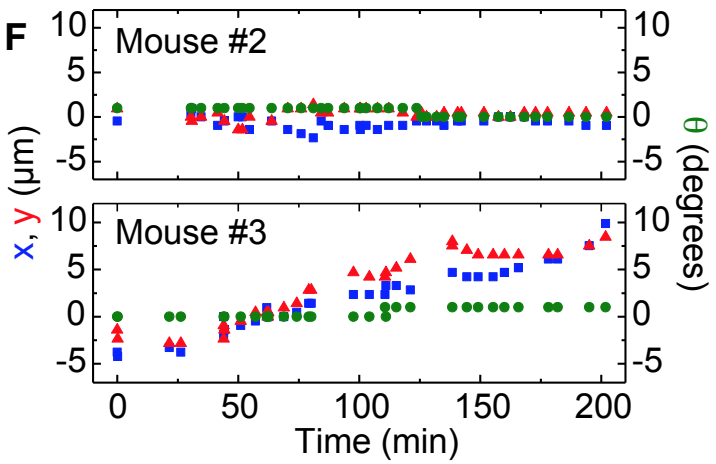
F
Mouse #2
Mouse #3
x, y (μm)
θ (degrees)
Time (min)

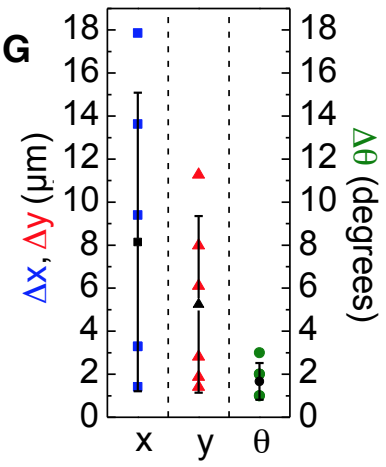
G
Δx, Δy (μm)
Δθ (degrees)
x
y
θ

Figure 5

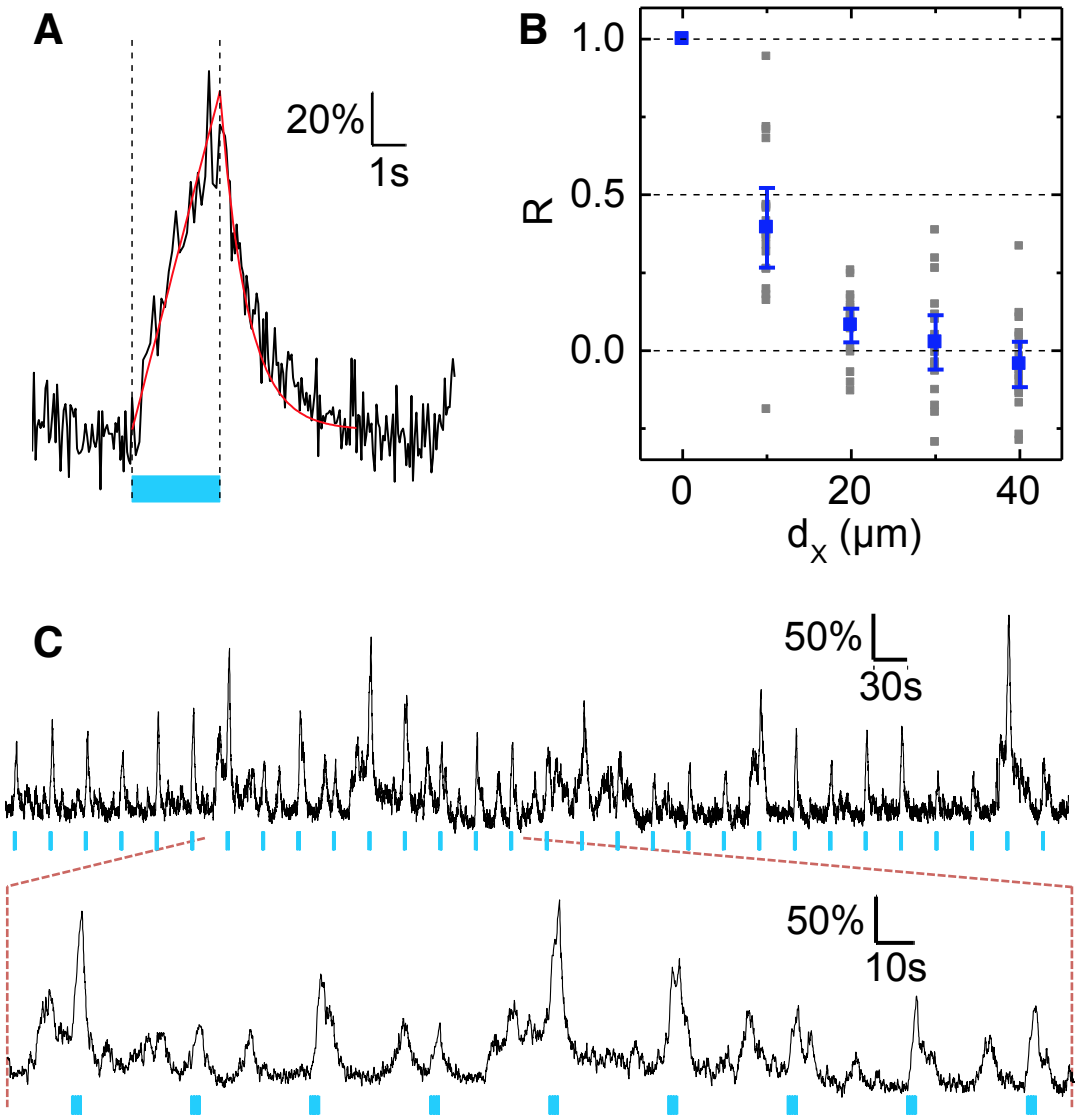

Figure 6